CryoTEMPO-EOLIS

Elevation Over Land Ice from Swath

Algorithm Theoretical Basis Document

Land Ice Elevation Thematic Point Product

Land Ice Elevation Thematic Gridded Product

Issue: 1.1

Date: 29th December 2021

Control Document

Prepared by :	Earthwave	
Issued by :		
Checked by :		
Approved by :		

Document Versions

Issue	Date	Author	Reason for change
1.0	8th Nov 2021	Carolyn Michael	First version of document
1.1	29th Dec 2021	Martin Ewart	Updated and reviewed

1. Table of Contents

1. Introduction **5**

1.1 Purpose and Scope *5*

1.2 Reference Documents *5*

1.3 Reference Websites *6*

2. Scientific Background **7**

3. Point product **7**

3.1 Introduction *7*

3.2 Algorithm description *7*
3.2.1 Swath Processing 7
3.2.2 Uncertainty Score 7

3.3 Input data and algorithm output *9*
3.3.1 Input data 9
3.3.2 Algorithm output 10

3.4 Choice of Uncertainty Score Variables *12*

3.5 Capabilities and known limitations *14*
3.5.1 Phase Model Correction 14

4. Gridded product **15**

4.1 Introduction *15*

4.2 Algorithm description *15*
4.2.1 Gridding methodology 15
4.2.2 Median filter 16

4.3 Input data and algorithm output *16*
4.3.1 Gridding method 16
4.3.2 Uncertainty score 17

4.4 Elevation change timeseries derived from gridded products *19*

4.5 Capabilities and known limitations *21*
4.5.1 Coverage 21
4.5.2 LRM Boundary 23

List of acronyms

DEM	Digital Elevation Model
EO	Earth Observation
EOLIS	Elevation Over Land Ice from Swath
ESA	European Space Agency
FTP	file transfer protocol
GDAL	Geospatial Data Abstraction Library
GS	Ground Segment
InSAR	Interferometric Synthetic Aperture Radar
LRM	Low Resolution Mode of the CryoSat-2 radar sensor
NetCDF	Network Common Data Form (binary file format)
OIB	Operation Ice Bridge
PDGS	Payload Download Ground Segment
POCA	Point-Of-Closest-Approach
SARIn	The CryoSat-2 SAR Interferometry mode
STSE	Science, Technology, Society and Environment education
UoE	University of Edinburgh
UTC	Coordinated Universal Time
XML	Extensible Mark-up Language

1. Introduction

1.1 Purpose and Scope

This document contains the Algorithm Theoretical Basis for the ESA CryoTEMPO EOLIS project. The ATBD describes the scientific background and principle of the algorithms, their expected or known accuracy and performance, the input and output data, as well as capabilities and limitations. The CryoTEMPO-EOLIS consists of two distinct products;

1) a point product containing a cloud of elevations with an associated uncertainty in geo spatial units; and
2) a gridded product containing a spatial interpolation of the point product onto a uniform grid of elevation and uncertainty.

This product covers three main regions: Antarctic ice sheet, Greenland ice sheet and Glacier regions. The Glacier regions cover Iceland, Svalbard, Arctic Canada, Russian Arctic, Alaska, Southern Andes, High Mountain Asia, peripheral glaciers in Antarctica and peripheral glaciers in Greenland.

1.2 Reference Documents

ESA (2019), CryoSat Baseline-D Product Handbook, https://earth.esa.int/documents/10174/125272/CryoSat-Baseline-D-Product-Handbook

German Aerospace Center (DLR) (2018) TanDEM-X - Digital Elevation Model (DEM) - Global, 90m. doi: https://doi.org/10.15489/ju28hc7pui09

Gourmelen, N. et al. (2018) 'CryoSat-2 swath interferometric altimetry for mapping ice elevation and elevation change', Advances in Space Research. Pergamon, 62(6), pp. 1226–1242. doi: 10.1016/J.ASR.2017.11.014.

Slater, T., Lawrence, I. R., Otosaka, I. N., Shepherd, A., Gourmelen, N., Jakob, L., Tepes, P., Gilbert, L., and Nienow, P. (2021), Review article: Earth's ice imbalance, The Cryosphere, 15, 233–246, https://doi.org/10.5194/tc-15-233-2021

Jakob, L., Gourmelen, N., Ewart, M., and Plummer, S. (2021), Spatially and temporally resolved ice loss in High Mountain Asia and the Gulf of Alaska observed by CryoSat-2 swath altimetry between 2010 and 2019, The Cryosphere, 15, 1845–1862, https://doi.org/10.5194/tc-15-1845-2021

Helm, V., Humbert, A. and Miller, H. (2014) 'Elevation and elevation change of Greenland and Antarctica derived from CryoSat-2', *Cryosphere*, 8(4), pp. 1539–1559. doi: 10.5194/tc-8-1539-2014.

Howat, I. M. et al. (2019) 'The Reference Elevation Model of Antarctica', The Cryosphere, 13, pp. 665–674. doi: https://doi.org/10.5194/tc-13-665-2019.

Jarvis A., H.I. Reuter, A. Nelson, E. Guevara, (2008), 'Hole-filled seamless SRTM data V4', International Centre for Tropical Agriculture (CIAT), available from https://srtm.csi.cgiar.org.

Krabill, W. B. (2016) IceBridge ATM L2 Icessn Elevation, Slope, and Roughness, Version 2. NASA National Snow and Ice Data Center Distributed Active Archive Center, Boulder, Colorado USA. http://nsidc.org/data/ilatm2.

Malicke (2021) 'SciKit GStat'. https://scikit-gstat.readthedocs.io/en/latest/userguide/variogram.html

McMillan, M. et al. Rapid dynamic activation of a marine-based Arctic ice cap. Geophys. Res. Lett. 41, 8902–8909 (2014)

Dunse, T. et al. (2015) Glacier-surge mechanisms promoted by a hydro-thermodynamic feedback to summer melt. The Cryosphere 9, 197–215

Foresta, L. et al. (2016) Surface elevation change and mass balance of Icelandic ice caps derived from swath mode CryoSat-2 altimetry. Geophys. Res. Lett. 43, 12,138-12,145

Wouter, B., Gardner, A. S., Moholdt, G. Global Glacier Mass Loss During the GRACE Satellite Mission (2002-2016). *Frontiers in Earth Science* **7**, (2019). https://doi.org/10.3389/feart.2019.00096

Hugonnet, R., McNabb, R., Berthier, E. *et al.* Accelerated global glacier mass loss in the early twenty-first century. *Nature* **592,** 726–731 (2021). https://doi.org/10.1038/s41586-021-03436-z

Porter, C. et al. (2018) ArcticDEM, Harvard Dataverse, V1. doi: https://doi.org/10.7910/DVN/OHHUKH.

Recchia, L. et al. (2017) 'An Accurate Semianalytical Waveform Model for Mispointed SAR Interferometric Altimeters', IEEE Geoscience and Remote Sensing Letters, 14(9), pp. 1537–1541. doi: 10.1109/LGRS.2017.2720847.

Smith, B., H. A. Fricker, A. Gardner, M. R. Siegfried, S. Adusumilli, B. M. Csathó, N. Holschuh, J. Nilsson, F. S. Paolo, and the ICESat-2 Science Team. 2021. ATLAS/ICESat-2 L3A Land Ice Height, Version 4. [ATL06]. Boulder, Colorado USA. NASA National Snow and Ice Data Center Distributed Active Archive Center. doi: https://doi.org/10.5067/ATLAS/ATL06.004. [Date Accessed:12th November 2021].

Wingham, D. J. et al. (2004) 'The mean echo and echo cross product from a beamforming interferometric altimeter and their application to elevation measurement', IEEE Transactions on Geoscience and Remote Sensing, 42(10), pp. 2305–2323. doi: 10.1109/TGRS.2004.834352.

1.3 Reference Websites

CryoTEMPO-EOLIS Project Website: http://cryotempo-eolis.org/

CryoTOP Evolution: https://cryotop-evolution.org/

ESA CryoSat-2 Data Download: https://science-pds.cryosat.esa.int/

Operation IceBridge: https://nsidc.org/data/icebridge/

Arctic DEM: https://www.pgc.umn.edu/data/arcticdem/

REMA DEM: https://www.pgc.umn.edu/data/rema/

SRTM DEM: https://srtm.csi.cgiar.org/

2. Scientific Background

Global ice loss has been increasing over the past decades, with large contributions from glaciers, as well as from the two ice sheets (Slater *et al.*,2021). CryoSat-2's primary mission objectives are to monitor the changes affecting the world's sea-ice and large ice sheets to quantify thickness, mass trends and the contribution to sea-level change. In practice, CryoSat's revolutionary interferometric design has allowed several technical breakthroughs and led to the application of radar altimetry to environments that were previously unforeseen. The interferometric mode of CryoSat-2 can be exploited to produce wide 5km swaths of elevations at spatial resolution of 500m for each satellite pass, this is a tenfold increase in resolution from historical radar altimetry with up to two orders of magnitude more data points compared to those from Point-Of-Closest-Approach (POCA) data alone (Gourmelen *et al.*, 2018).

Following on from the early demonstration of the technique and of its potential impact, the "CryoSat ThEMatic PrOducts - SWATH Cryo-TEMPO" project (CryoTEMPO-EOLIS) consolidates the research and development undertaken during the CryoSat+ CryoTop / CryoTop evolution ESA STSE projects (Gourmelen *et al.*, 2018) and the CryoSat+ Mountain Glaciers project (Jakob *et al.*, 2021) into operational products. The purpose of the thematic products is to make the data available to the wider scientific community in a form that does not require a detailed understanding of the sensor used and extensive processing. This product allows users to perform analysis using swath data, besides providing an uncertainty metric on which to filter the data to a desired precision.

3. Point product

3.1 Introduction

The CryoTEMPO-EOLIS point product is a set of high quality CryoSat swath altimetry point data with uncertainty metrics applied. This product is designed to be user-friendly; for use by non-altimetry experts. The point products cover the following regions: Antarctic and Greenland ice sheets and peripheral glaciers, as well as the ice caps and glaciers in Iceland, Svalbard, Alaska, Arctic Canada, Russian Arctic, Southern Andes and High Mountain Asia.

3.2 Algorithm description

3.2.1 Swath Processing

Swath processing of CryoSat-2 data has been detailed as part of the CryoSat+ CryoTop / CryoTop evolution ESA STSE projects (Gourmelen *et al.*, 2018).

3.2.2 Uncertainty Score

Firstly, for each region, the swath data is compared to another point elevation reference dataset (see Section 2.3.1):

$$\Delta E = E_{swath} - E_{ref}$$

where E_{swath} and E_{ref} are the swath and reference elevations respectively joined within a 10-day time window and 50m radius. This gives an estimate of the swath error value, however, it has to be noted that the differences, ΔE, are made up of errors in swath dataset, errors in the reference dataset, penetration differences between E_{swath} and E_{ref}, errors due to variation in topography, as well as other systematic differences meaning that it cannot directly be used as a measure of data uncertainty.

Over glacier regions, where variation of topography can be high, a slope correction is applied to the elevation difference measurements, using a reference Digital Elevation Model (DEM) (see Section 2.3.1):

$$corr = \mathrm{DEM}(x_{swath}, y_{swath}) - \mathrm{DEM}(x_{ref}, y_{ref})$$

$$\Delta E_{corr} = \Delta E - corr$$

where $\mathrm{DEM}(x_{swath}, y_{swath})$ and $\mathrm{DEM}(x_{ref}, y_{ref})$ are the DEM elevations at the nearest neighbour swath and reference dataset coordinates. Applying this correction minimises the error due to variation in topography.

In order to minimise these other differences in elevation between the swath and reference datasets within the uncertainty score, the standard deviation of the elevation difference is calculated. To calculate the standard deviation, the sample data is binned using several variables. For all regions other that those in High Mountain Asia, the following six variables (see Section 3.4) are used:

Power in Decibels	As defined in the CryoSat-2 Product Handbook (ESA, 2019)
Coherence	As defined in the CryoSat-2 Product Handbook (ESA, 2019)
Distance to POCA	Distance in metres between the Swath observation and the POCA derived using the TFRMA retracker (Helm, Humbert and Miller, 2014).
Along Track Slope	Slope is calculated along the track at a length scale of 400m where slope is defined as change in elevation in metres between 200m in front and 200m behind the observation divided by 400m.
Across Track Slope	Slope is calculated across the track at a length scale of 1600m where slope is defined as change in elevation in metres between 800m to the left and 800m to the right of the observation divided by 1600m.
Roughness	Calculated from the reference DEM using the GDAL library function “gdaldem roughness”.

A six-dimensional cube consisting of each variable binned into 6 equal volume bins is generated. The data is sampled using every bin combination across all variables resulting in 6^6 (= 46,656) bins (quality bins). A set of quality bins are calculated separately for Antarctic Ice Sheet, Greenland Ice Sheet, and then all Glacier regions apart from High Mountain Asia. For High Mountain Asia the Distance to POCA bin was removed as sample data size for the uncertainty calculation was not sufficiently large enough, instead the data was split into 5 equal volume bins resulting in 5^5 (= 3,125) quality bins.

The standard deviation is calculated from the binned sampled data which gives a range of high to low quality combinations of variables. To ensure that the sample size in each bin is considered, the upper bound of the confidence interval of the standard deviation is calculated:

$$\sigma \leq s\sqrt{\frac{n-1}{\chi^2_{1-\alpha/2}}}$$

where s is standard deviation of the sample, n is sample size, χ^2 is the Chi-square distribution and α is set to 0.05 to give a one-sided 97.5% confidence interval. This upper estimate of the standard deviation is defined as the uncertainty value for each of the quality bin combinations.

These quality bins are then used to apply to each individual observation to estimate its uncertainty, given the data points 6 variable values. It should be noted that the uncertainty metric provided is not a guarantee that the elevation is accurate to within the uncertainty score given, moreover it means for the test sample data, that there is a 97.5% confidence that the true standard deviation of the data will be less than the uncertainty score for a combination of variables. In other words, it is a conservative estimate of the uncertainty for a point but does not guarantee the point is not an outlier.

3.3 Input data and algorithm output

3.3.1 Input data

Before the uncertainty score is calculated, the following baseline filters are applied to the swath elevation data to remove any weak signal and poor-quality data:

- Power in Decibels > -160 dB (Antarctic and Greenland ice sheets, Glacier regions (excluding High Mountain Asia)), >-175 dB (High Mountain Asia)
- Power Scaled > 100
- Coherence > 0.6 (Antarctic and Greenland ice sheets), > 0.5 (Glacier regions)
- Absolute difference to a reference DEM <100m
- Median absolute deviation of swath compared to reference DEM < 6m (Antarctic and Greenland ice sheets), <20m (Glacier regions)

These filters were chosen based on comparisons to reference datasets (such as OIB and ICESat2) to find values which minimised the standard deviations of the elevation difference whilst also maintaining an optimal volume of points. The power in decibels filter was loosened over High Mountain Asia as due to topography the mean power of the distribution is much lower. For all glacier regions the Median absolute deviation of elevation difference was on average observed to be higher, especially in steep terrain, and so this filter was also loosened to 20m.

As a reference DEM, the Arctic DEM mosaic is used for Greenland, Iceland, Svalbard, Russian Arctic, Arctic Canada and Alaska (Porter *et al.*, 2018), the REMA DEM mosaic for Antarctica (Howat *et al.*, 2019), and TanDEM-X DEM for Southern Andes and High Mountain Asia (German Aerospace Center (DLR), 2018). If there is not a TanDEM-X value available for a location, then the SRTM DEM is used (Jarvis et al, 2008).

To calculate elevation difference to the reference dataset, all swath data between 2011 and 2016 are spatially joined with OIB data (Krabill, 2016) within a 10 day time window and 50m radius for the uncertainty calibration of Antarctic and Greenland ice sheets. Whereas all swath data between October 2018 and December 2020 is spatially joined with ICESat2 data (Smith *et al.*, 2021) within a 10 day time window and 50m radius over the glacier regions.

For the High Mountain Asia quality bins, a combination of all joined data over High Mountain Asia and Alaska is used which is roughly an equal split across both regions. The Alaska data was used to increase data volume for the uncertainty calculation.

For the Antarctic and Greenland ice sheet products, any data that sits outside of the 95th percentile of the Along Track slope, Across Track slope and Roughness values is removed, meaning any extreme values are discarded. This is not applied over the glacier regions to avoid coverage loss as topography is more variable.

3.3.2 Algorithm output

As output, the algorithm provides a six-dimensional cube consisting of the six variables binned into six equal volume buckets with associated 97.5% upper one-sided confidence bound for each combination (Table 1). For each swath point, the associated variables are matched to the bin definitions and the estimated uncertainty score for that bin is assigned to the swath point.

Table 1: Definition of buckets for Antarctic ice sheet, Greenland ice sheet, glacier regions and High Mountain Asia. Each bucket is between two bin edges, e.g. 0-1, 1-2 …. 5-6.

Antarctica

Bin Edge	Power [dB]	Coherence	Roughness	Slope Across	Slope Along	Distance To POCA [m]
0	-160.00	0.600	0.00	-0.0351	-0.0353	0
1	-154.68	0.778	0.66	-0.0114	-0.0088	4,959
2	-152.17	0.853	1.41	-0.0045	-0.0025	6,541
3	-150.09	0.899	2.35	-0.0009	0.0000	7,512
4	-147.93	0.931	3.65	0.0006	0.0028	8,589
5	-145.23	0.956	5.61	0.0052	0.0091	10,097
6	0.00	1.000	11.80	0.0351	0.0353	21,033

Greenland

Bin Edge	Power [dB]	Coherence	Roughness	Slope Across	Slope Along	Distance To POCA [m]
0	-160.00	0.600	0.00	-0.0349	-0.0348	0
1	-154.69	0.838	1.51	-0.0149	-0.0106	4,098
2	-152.09	0.901	2.54	-0.0078	-0.0041	5,952
3	-149.90	0.933	3.62	-0.0028	-0.0001	7,134
4	-147.61	0.953	4.97	0.0030	0.0037	8,387
5	-144.76	0.968	6.91	0.0118	0.0098	10,043
6	0.00	1.000	13.26	0.0349	0.0348	21,582

Glacier Regions

Bin Edge	Power [dB]	Coherence	Roughness	Slope Across	Slope Along	Distance to POCA [m]
0	-160.00	0.500	0.00	-0.5255	-0.9696	0
1	-157.97	0.783	3.68	-0.0243	-0.0240	301
2	-155.93	0.877	5.16	-0.0123	-0.0103	1079
3	-153.82	0.922	6.69	-0.0004	0.0002	2387
4	-151.48	0.950	8.65	0.0116	0.0108	4263
5	-148.36	0.970	11.97	0.0242	0.0247	6654
6	0.00	1.000	198.47	0.6972	0.6952	23568

High Mountain Asia

Bin Edge	Power [dB]	Coherence	Roughness	Slope Across	Slope Along
0	-175.00	0.500	0.00	-0.6998	-1.9517
1	-168.66	0.642	7.89	-0.0537	-0.0646
2	-166.40	0.758	14.11	-0.0114	-0.0143
3	-163.67	0.857	23.64	0.0142	0.0146
4	-159.08	0.934	40.25	0.0517	0.0628
5	0.00	1.000	495.72	0.8218	1.0801

3.4 Choice of Uncertainty Score Variables

For each variable used in the uncertainty calculation there is a clear link between the value of the variable and the uncertainty score (Figure 1).

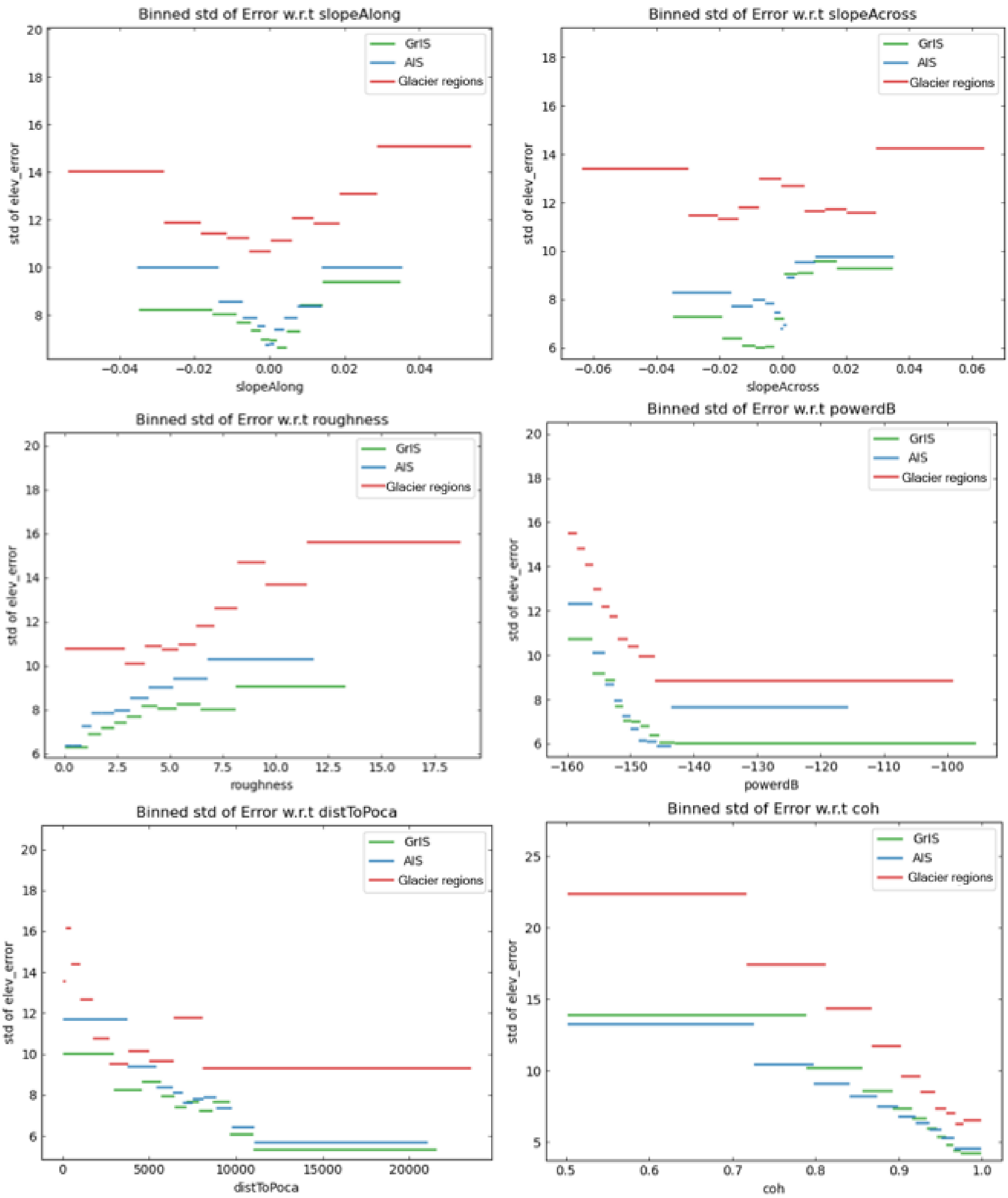

Figure 1: Standard deviations of equal volume bins of points for each variable for glacier regions (red), compared to those over Greenland Ice Sheet (green) and Antarctic Ice Sheet (blue). The distributions follow a similar pattern for most variables, but the standard deviation is higher for the glaciers regions.

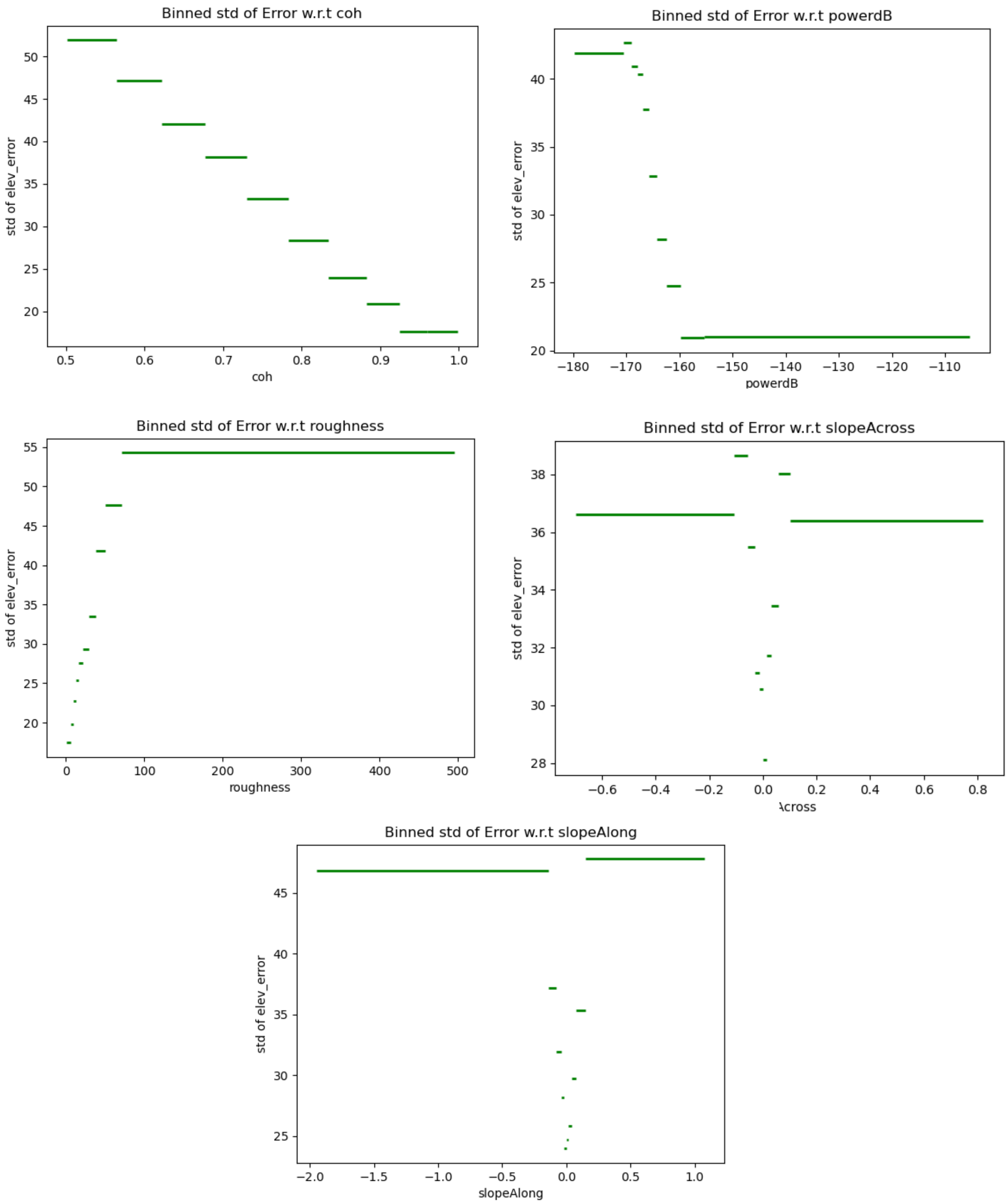

Figure 2: Standard deviations of equal volume bins of points for each variable for High Mountain Asia. The distributions follow a similar pattern for most variables when compared the Antarctic and Greenland ice sheets and the glacier regions, but the standard deviation is higher.

Higher slope of the underlying terrain results in a higher uncertainty score, this is observed for *slopeAlong* and *slopeAcross*. Swath data where the power in decibels is high results in a lower uncertainty score, with the opposite applying for low power data points. Similar linear correlations are observed for coherence where high coherence data has a low uncertainty score and low coherence data has a higher uncertainty score. The same relationship is recorded for the distance to the nearest POCA point with swath points further from the POCA having a low uncertainty score. Finally, we see that data where the roughness, a measure of the irregularity of the surface, is low then the associated uncertainty score is also low, and higher roughness results in higher uncertainties.

3.5 Capabilities and known limitations

3.5.1 Phase Model Correction

Product quality is affected by phase model accuracy (Wingham *et al.*, 2004; Recchia *et al.*, 2017), causing residual elevation slopes in the across track direction. This effect is predominantly observed in areas where the surface is relatively flat. We mitigate this effect using a simple empirical model. It corrects the first order effect, greatly reducing the features in the product, however residuals of a few metres in amplitude are still observed. Future versions of the CryoTEMPO-EOLIS products will incorporate an improved physical phase model.

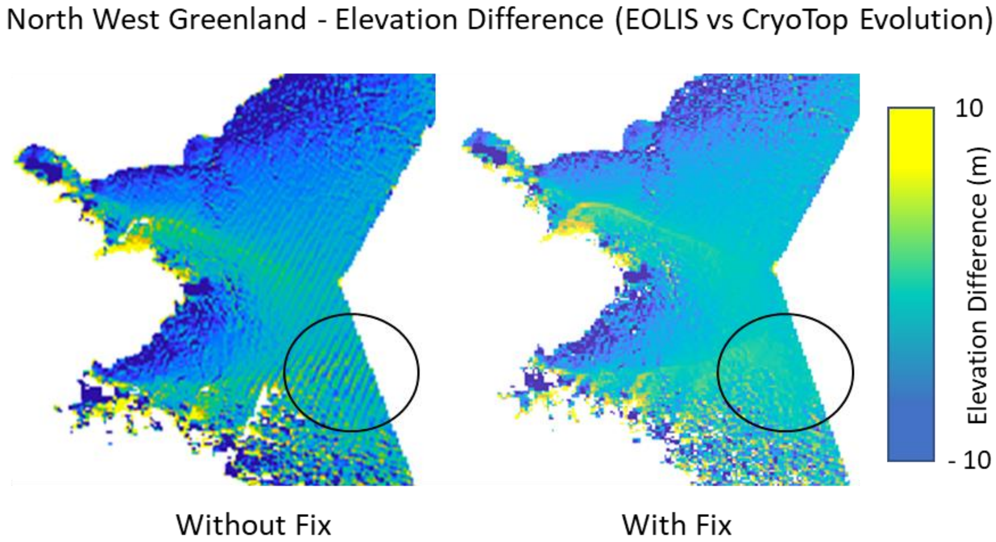

Figure 3: Example of improvement in the DEM in North West Greenland. Without the correction, the flat areas inland at the centre right of the image shows a striping effect in elevation difference when compared to a reference DEM. This is particularly prominent in the highlighted circle but happens throughout the flat region. However, with the fix, there is a more consistent elevation difference when compared to a reference DEM.

4. Gridded product

4.1 Introduction

The CryoTEMPO-EOLIS gridded products are monthly DEMs that allow users to have instant access to gridded and averaged point data at 2km spatial resolution. The CryoTEMPO-EOLIS DEMs are a valuable tool to monitor changes in topography at monthly temporal resolution. These products cover Antarctic and Greenland ice sheets, as well as Austfonna ice cap in Svalbard and Vatnajökull ice cap in Iceland.

4.2 Algorithm description

4.2.1 Gridding methodology

The gridded products are generated on a monthly basis, using the CryoTEMPO-EOLIS point product data, with each monthly DEM using a 3-month overlapping temporal window which is centred on the middle of the publication month.

Two separate methods are used for the ice sheets and ice caps. The gridding method used for Austfonna and Vatnajökull ice caps takes findings from Jakob et al. (in review) to remove noise due to topography. This method will be used over Greenland and Antarctic ice sheets in the next phase of the project.

Greenland and Antarctic ice sheet DEMs

There are multiple phases in the construction of the gridded product from the point data, which are detailed below:

1) **Cluster removal:** The point data and the ESA POCA data are mapped onto a uniform 200m grid using the Inverse Distance Weighted interpolation algorithm.
2) **Padding:** The grid is padded with no data values for pixels that have no values.
3) **Filling:** The 200m gridded is interpolated using an inverse distance weighting algorithm with a maximum pixel distance of 1600m .
4) **Re-sampling**: The 200m grid is re-sampled to 2km using a cubic interpolation method.
5) **Masking of LRM and ice sheet:** a 2km raster mask is created that contains the region of interest of the product.
6) **Compute difference to reference DEM:** the median mask in the next step requires the difference of the gridded swath elevations to a reference DEM (DEMdiff) (see Section 4.3.1).
7) **Reduction of boundary noise and artefacts:** a median filter is applied iteratively 8 times to the gridded DEMdiff.

Vatnajökull and Austfonna glacier DEMs

A different gridding approach was implemented to account for a more complex topography (Jakob et al., in review). The new approach is as follows:

1) **Topography removal:** Topography is removed from the gridding by subtracting the reference DEM from the swath elevation measurements at a point level (DEMdiff).

2) **Median calculation:** For each 2km posting, all DEMdiff values within a 2km radius are combined using a median calculation to create a gridded DEMdiff.
3) **Padding:** The grid is padded with no data values for pixels that have no values
4) **Reduction of boundary noise and artefacts:** a median filter is applied iteratively 2 times to the gridded DEMdiff (see section below).
5) **Masking of LRM and Ice Sheet:** a 2km raster mask is created, containing the region of interest of the product.
6) **Topography retrieval:** the gridded DEMdiff is converted back to a DEM using the reference DEM.

4.2.2 Median filter

The CryoTEMPO-EOLIS DEM is adjusted using a median filter to exclude pixels that have large differences to reference DEM due to poor spatial coverage and to smooth pixels where there is good surrounding spatial coverage.

Firstly, using the DEMdiff, the median of each pixel with surrounding pixels within a 5x5 moving kernel is calculated. To ensure even spatial coverage, the median is only calculated where all four corners of the kernel are occupied with data.

The difference between this nearest neighbour median DEMdiff and the DEMdiff is calculated (MedDEMdiff), giving an indication of the local variation in elevation. The standard deviation (σ) of the differences is then calculated, which can be used as a threshold to identify outliers.

If the absolute difference is less than 3σ then the DEMdiff value remains unchanged, otherwise an adjustment value for that pixel is set to the corresponding MedDEMdiff value and then applied to the DEM.

This approach is applied iteratively, with each iteration the standard deviation will decrease providing a tighter threshold. However, where topography is more variable (i.e. glacier regions), this may reduce the magnitude of data, and therefore fewer iterations are used.

4.3 Input data and algorithm output

4.3.1 Gridding method

Greenland and Antarctic DEMs

The gridded product uses swath data points that have a maximum uncertainty of 7m as a quality filter. The ESA Baseline D POCA was added to improve coverage. There are POCA points which have a large elevation difference with the nearest swath point and the reference DEM. Only POCA points that have an absolute difference of <100m with the reference DEM e.g. Arctic DEM for Greenland and REMA for Antarctica are included.

Vatnajökull and Austfonna DEMs

The gridded product uses swath data products that have a maximum uncertainty of 20m as a quality filter. The ESA Baseline D POCA was not included as there was not an associated error for filtering of data to remove erroneous points which resulted in noise within the DEM. Moreover, no error from the POCA data could be propagated to calibrate the uncertainty score.

4.3.2 Uncertainty score

For Vatnajökull and Austfonna the point uncertainty is propagated to provide an uncertainty estimate of each pixel using the following equation:

$$\sigma_p = \sqrt{\sum_i^n \frac{1}{n^2}\sigma_i^2 + \sum_i^n \sum_{j(j\neq i)}^n \frac{1}{n^2}\rho_{ij}\sigma_i\sigma_j}$$

where:

σ_p = Uncertainty of a pixel

σ_i, σ_j = Uncertainty of individual points

ρ_{ij} = Spatial autocorrelation between 2 points

n = Number of points contributing to a pixel

This equation reduces to the standard error of the mean uncertainty if all points have 0 correlation. Conversely, if all points are 100% correlated, the uncertainty is the mean of the uncertainties, which is a maximum of 20m given the maximum uncertainty of points is 20m.

A semi-variogram is used to determine the spatial auto correlation ρ_{ij} based on the separation of the points. This semi-variogram is calculated using the Python SciKit GStat library.

For a sample of 50000 points spread across the whole of Vatnajökull and Austfonna semi-variograms are derived using a maximum lag of 5km with an even binning function, the a model and the Cressie estimator. Using the sill as an estimate for the covariance and the derived semi-variance, the estimated spatial auto-correlation as a function of distance between points is then calculated as:

$$\rho_{dist} = \frac{Sill - SV_{dist}}{Sill}$$

where:

ρ_{dist} = spatial auto-correlation for a given distance

SV_{dist} = Semi-variance for a given distance

A third order polynomial is then fit to the ρ_{dist} values between 0 and 5km to give an equation that can be used to estimate the spatial-autocorrelation.

$$\rho(x) = ax^3 + bx^2 + cx + d$$

where x is the distance between observations.

The following coefficients are determined:

Austfonna
a = -7.362538068835588e-12
b = 7.984907143327342e-08
c = -0.0003012011566802816

d = 0.4204838462111617

Vatnajökull
a = -8.114067346350161e-12
b = 9.524158216288018e-08
c = -0.0004014163183448419
d = 0.6320073140239348

Figure 4 shows the output for Vatnajökull in May 2015, displaying that for the applicable distance of 4000m, the autocorrelation is small and the maximum when the distance is 0m is 0.63.

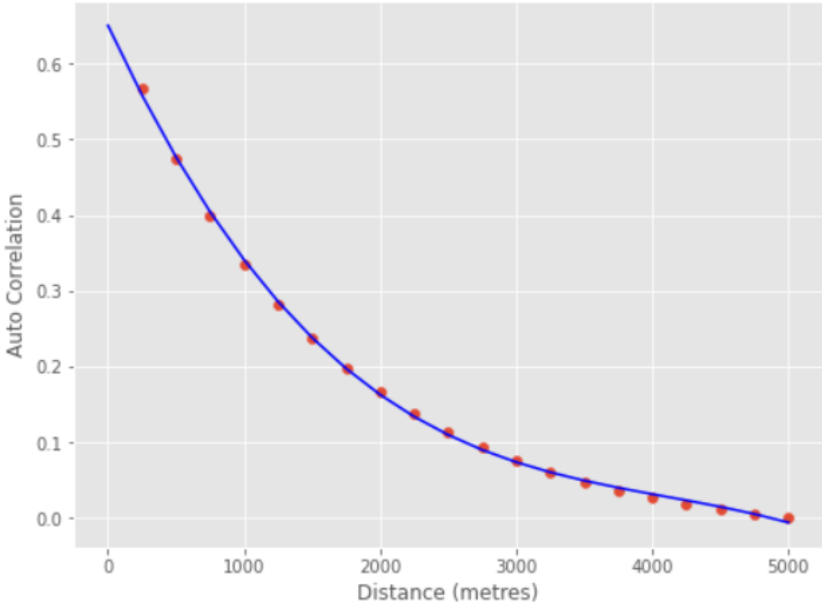

Figure 4: Spatial autocorrelation vs distance for Vatnajökull, generated for May 2015.

The consistency of the estimated spatial autocorrelation was validated by looking at the 4 quadrants of each region (North West, North East, South West and South East) in comparison to the autocorrelations for the whole region. In addition, different models and estimators were used from the SciKit GStat library and compared and a comparison of months between 2011, 2015 and 2019 was performed, to ensure a stable model. There was no more than a 10 percentage points difference in the comparisons, meaning that using a single polynomial per region is representative of the autocorrelation. Therefore, for consistency across a region it was decided to use one polynomial for a whole region. However, Austfonna and Vatnajökull are suitably different so that a different polynomial is needed for each.

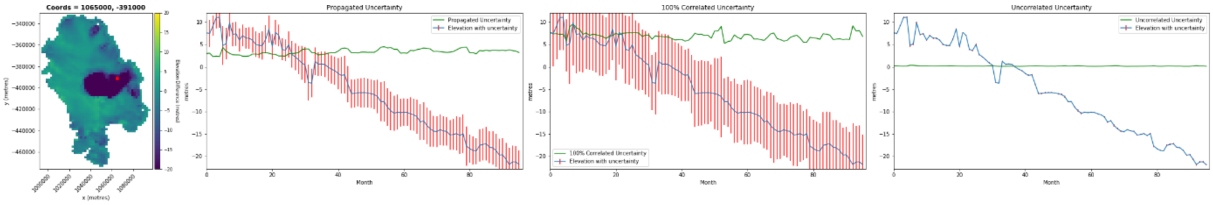

Figure 5: Example uncertainty and elevation plots over 9 years from 2011 to 2019 for a single location on Austfonna.

Using this in the uncertainty formula means that in general, low pixel uncertainties of order 1-2m are seen when there is a high volume of widely distributed points contributing to a pixel, and much higher uncertainties are observed when there is a low volume of points or narrowly distributed points.

This can be demonstrated by looking at a pixel over time. Outliers are clearly seen and highlighted by the uncertainty calculation.

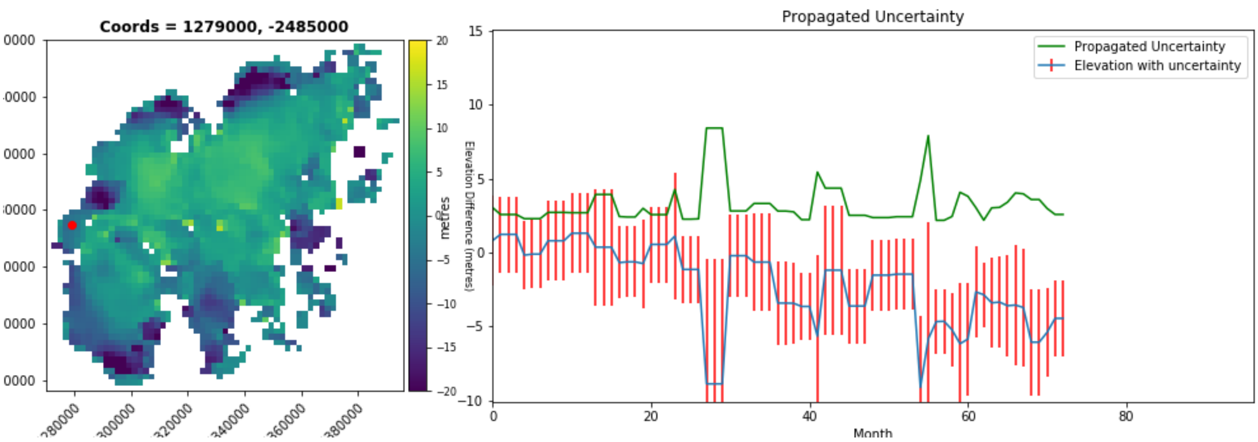

Figure 6: Example pixel near the edge of Vatnajökull. Outlier values clearly have higher uncertainty.

4.4 Elevation change timeseries derived from gridded products

Derived average monthly changes from CryoTEMPO-EOLIS DEMs over glaciers for Austfonna, Svalbard and Vatnajökull, Iceland in Figures 7 and 8 respectively. Figure 7 and 8 illustrate that the CryoTEMPO-EOLIS gridded products are able to capture well-known events such as the surge of Basin-3, associated with rapid ice loss from mid-2012 onwards (McMillan, M. *et al*. 2014, Dunse, T. *et al*. 2015), and the slow-down in ice loss in Iceland between 2013 and 2015 due to recent large winter accumulation (Foresta, L. *et al*., 2016). Both figures show trends comparable to other published studies using independent datasets (Wouters *et al.* 2019, Hugonnet *et al.* 2021).

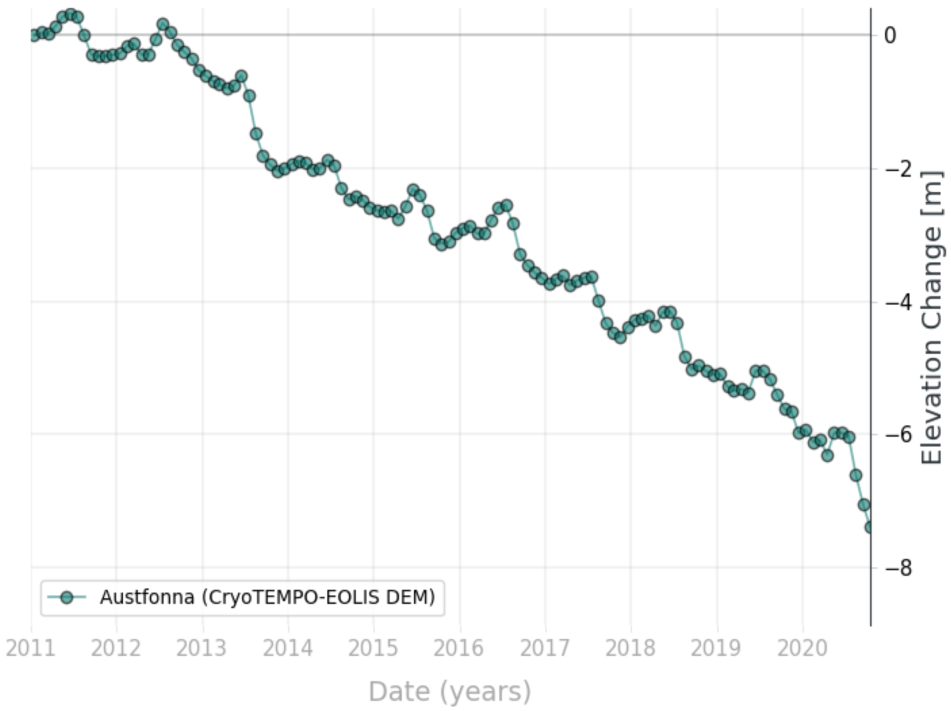

Figure 7: Cumulative monthly changes derived from the CryoTEMPO-EOLIS gridded products over Austfonna, Svalbard from 2011 to 2020.

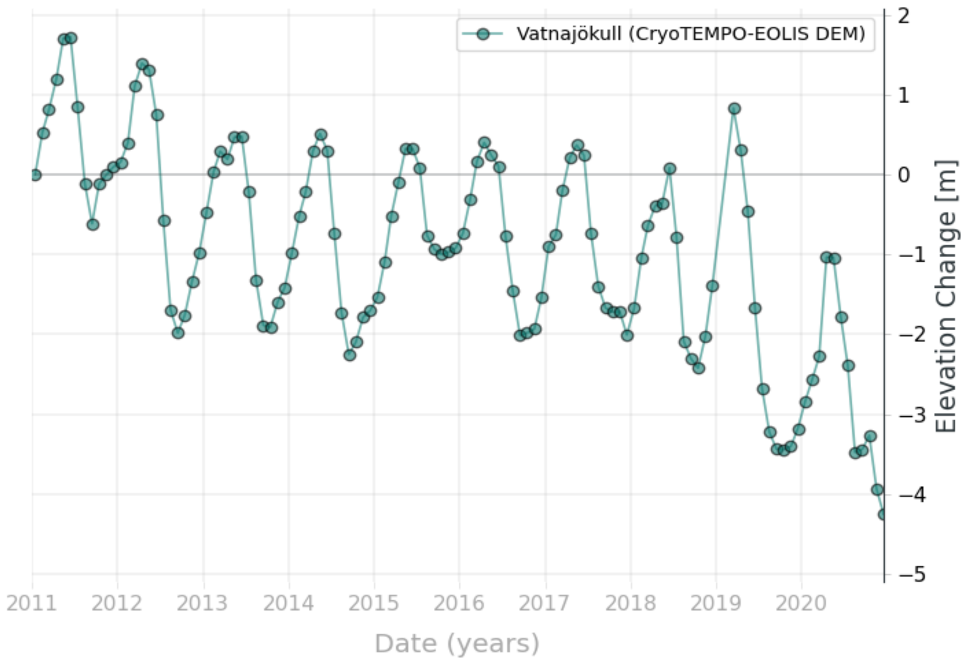

Figure 8: Cumulative monthly changes derived from the CryoTEMPO-EOLIS gridded products over over Vatnajökull, Iceland from 2011 to 2020.

4.5 Capabilities and known limitations

4.5.1 Coverage

Greenland and Antarctic ice sheets

CryoSat-2 coverage in south Greenland is less extensive than further north due to latitudinal change in orbit separation. Therefore, there are some areas with missing data for each monthly DEM. The decision to fix the product's resolution was a compromise to ensure sufficient spatial resolution and spatial coverage. The same to a lesser extent is seen in the west of Antarctica.

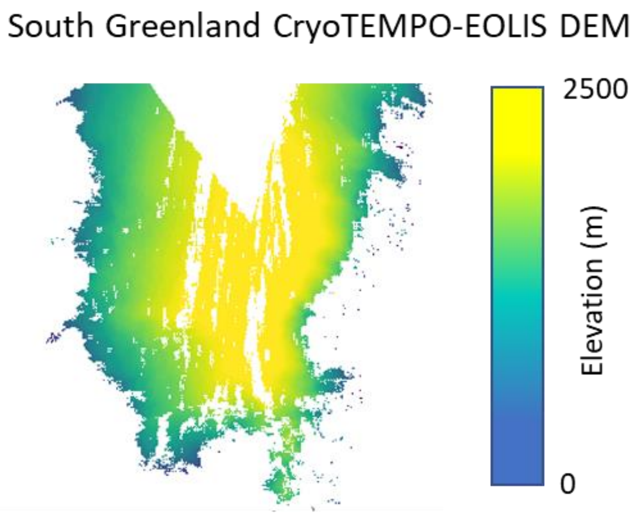

Figure 9: Example of coverages over south Greenland. Image taken from CryoTEMPO-EOLIS April 2015 DEM.

Austfonna and Vatnajokull ice caps

Coverage in Austfonna and Vatnajökull are extensive with monthly averages of 99% of total coverage for Austfonna and 85% of total coverage for Vatnajökull.

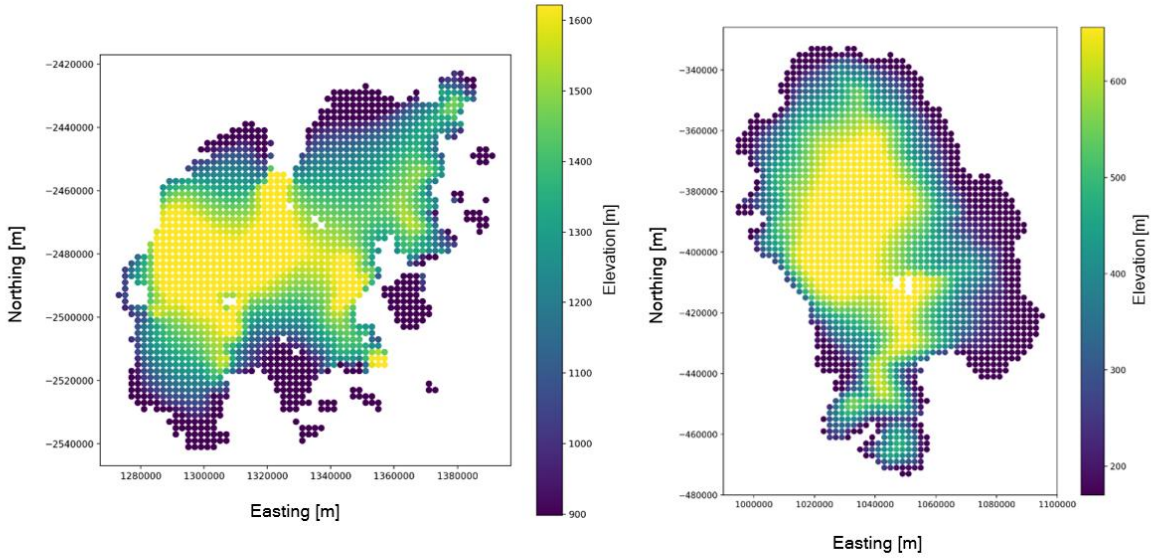

Figure 10: CryoTEMPO-EOLIS gridded products covering Vatnajökull (left) and Austfonna (right) for October 2021.

Coverage from August to November 2010, the first few months when CryoSat2 was first in operation, is slightly sparser for Vatnajökull with the total coverage ranging from 20-70%. The impact on Austfonna is negligible with the total coverage ranging from 88-97%.

4.5.2 LRM Boundary

Due to CryoSat-2 changing from LRM mode to SARIn mode at the LRM boundary, we observe higher level of noise near to the boundary. This results in higher level of missing data and residual noise in the gridded product.

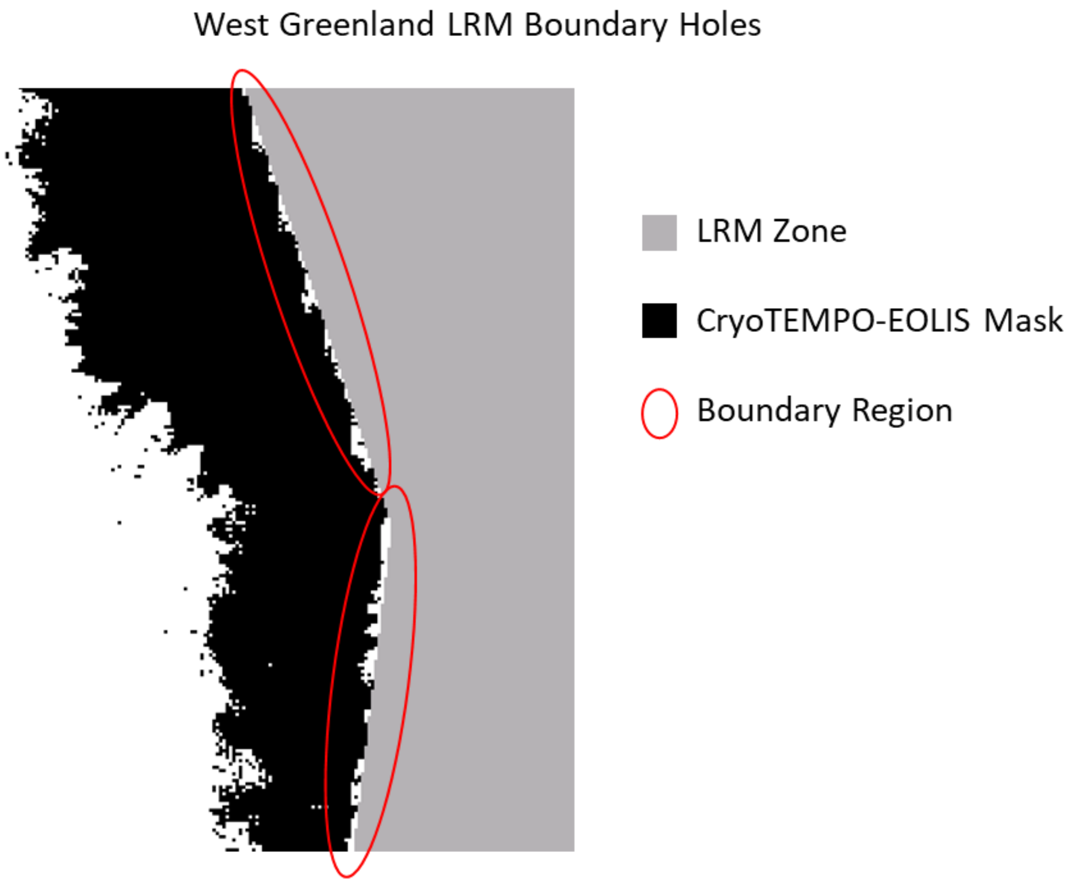

Figure 11: Example LRM boundary holes in West Greenland. The red ovals highlight holes in the CryoTEMPO-EOLIS DEM next to the LRM boundary due to poor quality data.